Intimate contact development during laser assisted fiber placement
Microstructure and effect of process parameters

Çelik, Ozan; Peeters, Daniël; Dransfeld, Clemens; Teuwen, Julie

DOI
10.1016/j.compositesa.2020.105888

Publication date
2020

Document Version
Final published version

Published in
Composites Part A: Applied Science and Manufacturing

Composites Part A 134 (2020) 105888

Contents lists available at ScienceDirect

Composites Part A

journal homepage: www.elsevier.com/locate/compositesa

Intimate contact development during laser assisted fiber placement: Microstructure and effect of process parameters

Ozan Çelik*, Daniël Peeters, Clemens Dransfeld, Julie Teuwen

Aerospace Manufacturing Technologies, Faculty of Aerospace Engineering, Delft University of Technology, Kluyverweg 1, Delft 2629HS, the Netherlands

ARTICLE INFO

Keywords:
A. Polymer-matrix composites (PMCs)
B. Microstructures
C. Process modeling
E. Automated fiber placement (AFP)

ABSTRACT

Intimate contact development under LAFP-specific thermal and mechanical boundary conditions/interactions and the effect of process parameters are investigated. One-layer, unidirectional strips of CF/PEKK material were placed with different process parameters on a flat tool surface to create different intimate contact conditions. The concept of *effective intimate contact*, which is based on the resin content at the surface, is introduced and a methodology to measure it from surface micrographs is provided. Degree of effective intimate contact measured from the samples was compared with the existing intimate contact models. The temperature history in the compaction zone was estimated with a finite element model and pressure sensitive films were used to determine the compaction pressure. It is shown that in addition to the squeeze flow mechanism, which is the base for the current intimate contact models, through-thickness percolation flow of the resin needs to be considered to explain the effective intimate contact development.

1. Introduction

Thermoplastic composites (TPC) have drawn significant interest in the aerospace industry for their infinite shelf life, high fracture toughness, chemical and solvent resistance, weldability and recyclability [1–3]. Automated fiber placement (AFP) has become a promising manufacturing solution for TPC, providing reduction in labor time per component, lower material scrap rates and higher repeatability [4]. In modern laser assisted fiber placement (LAFP) systems, a laminate is built by heating the surface of the tape and substrate with a laser heat source pointed towards the nip point and compacting with a flexible roller as shown in Fig. 1.

Due to the re-melting capability of thermoplastic polymers, in-situ consolidated (i.e., without a post-consolidation step in an autoclave, oven or press) structures can be manufactured with the LAFP process. This aspect of the technology is especially appealing since significant capital investment and operating costs related to post-consolidation can be saved if sufficient part quality with a feasible processing speed is achieved. In order to achieve this goal, extensive research has been conducted in the last decades to understand the mechanisms which play a role at the heating, compaction and cooling phases of the process [5–14].

The compaction phase is especially critical since two subsequent plies consolidate only with the pressure supplied by the compaction roller. Intimate contact development is the first step of consolidation and affects several aspects during the process which significantly influence the properties of the final structure. Firstly, bond strength formation between subsequent plies requires intimate contact development between surfaces. Bonding is driven by diffusion and entanglement of polymer molecules across the interface through reptation [15]. This mechanism is active only at the locations which are in intimate contact [16]. Secondly, inter-laminar void content in the final structure is a direct result of intimate contact development. Such voids act as crack initiation points and reduce the mechanical performance of the final product, especially inter-laminar shear, compression and transverse tensile strength and fatigue life [17]. Finally, heat transfer might be reduced at the ply interfaces due to incomplete intimate contact [10,18]. The effect of reduced heat transfer on the temperature history influences all temperature related phenomena during LAFP, e.g. crystallinity, healing, void compaction/decompaction and residual stresses. Understanding how intimate contact develops during LAFP is therefore an important step for linking the process parameters to the final quality of the parts.

The common approach to explain how intimate contact develops during thermoplastic composite processing has been based on the squeeze flow of the surface asperities. Such models combine the compaction force, an idealized description of the composite surface and the temperature-dependent homogenized viscosity of the composite

* Corresponding author.
E-mail address: ozan.celik@tudelft.nl (O. Çelik).

https://doi.org/10.1016/j.compositesa.2020.105888
Received 3 December 2019; Received in revised form 10 February 2020; Accepted 21 March 2020
Available online 06 April 2020

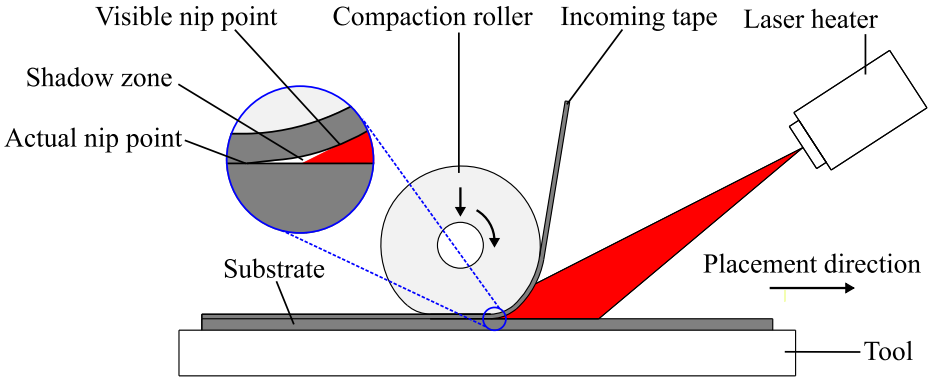

Fig. 1. Working principle of LAFP systems. (For interpretation of the references to color in this figure legend, the reader is referred to the web version of this article.)

material to find the degree of intimate contact given the temperature and pressure history of the process. Using this approach, several models were proposed for intimate contact development. The first model was proposed by Dara and Loos for isobaric and isothermal conditions [19]. The squeeze flow mechanism was justified by the high viscosity of the thermoplastic polymers at melting temperature. They modeled the composite surface as a collection of rectangular elements with non-uniform height and width, approximated by a 2-parameter Weibull distribution. Lee and Springer [20] followed a similar rationale but simplified the surface representation with uniform rectangles. Mantell and Springer [21] extended this model for non-uniform pressures and temperatures, which is more suitable for automated fiber placement or winding. Yang and Pitchumani suggested that the asperities in the thermoplastic composite surfaces exhibit fractal characteristics and proposed a surface representation with a fractal Cantor set [22].

These models have been extensively used to predict intimate contact development for the AFP process [23–26]. However, limited prediction accuracy was reported for modern systems with laser heaters [26–28]. This raises the question of whether the squeeze flow mechanism with homogenized material assumption is completely suitable to explain intimate contact development during LAFP. Rapid heating to high processing temperatures (370–400 °C for carbon fiber reinforced polyetherketoneketone (CF/PEKK) [29] and carbon fiber reinforced polyetheretherketone (CF/PEEK) [30] tapes) without pressure application and very short compaction times (usually between 0.01 and 0.3 s depending on the deformation of the compaction roller and the placement speed) are distinctive features of LAFP. Moreover, heating above the melting temperature of the resin material without pressure application results in a fiber-rich and rough surface until the tape reaches the nip point [31]. Considering that a significant portion of the tapes already has a resin-poor surface in their original state such as the one shown in Fig. 2 and the microstructure of the tape changes during the heating phase, intimate contact development might not be adequately described with the squeeze flow mechanism. Intimate contact models mentioned above were validated by press-consolidated samples with compaction times orders of magnitude higher than typical compaction times for LAFP, which might suppress the effect of non-uniform microstructure at the surface. Considering the state-of-the-art literature, how intimate contact develops at short time spans typically found in the LAFP process, taking the microstructural changes due to laser heating into account, is still an open question.

Another reason for the lack of knowledge about the mechanisms involved in intimate contact development is how the degree of intimate contact is measured. The degree of intimate contact was measured mostly at the interfaces between the plies [19,22,23,32], although the available intimate contact models consider flattening of a single composite surface against a rigid surface. There is only one study where the predicted intimate contact was compared with the surface of press-consolidated individual tapes [20]; however, the details of how the degree of intimate contact was measured was omitted. Moreover, the final state of the composite interface contains little information about the process of intimate contact development during compaction. Therefore, a more detailed analysis of the intimate contact development on a single tape under LAFP conditions is required.

The aim of this paper is therefore to understand the intimate contact development mechanism under LAFP-specific thermal and mechanical boundary conditions/interactions. Specifically, the following questions will be addressed: How can the degree of intimate contact be quantified considering the inhomogeneity of the composite surface? What is the effect of LAFP process parameters on intimate contact development? Can the squeeze flow mechanism fully explain the intimate contact development during LAFP?

To answer these questions, one-layer samples were prepared with a LAFP machine with different process parameters. The final degree of

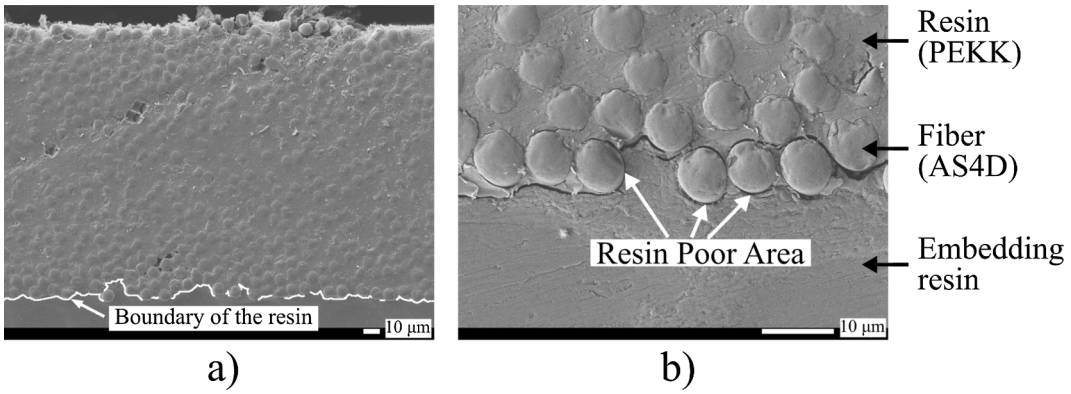

Fig. 2. Scanning Electron Microscope images of the cross-section of the unprocessed CF/PEKK tape. (a) Moderate magnification (450×), resin level on the surface is indicated with a white boundary. (b) High magnification (2000×), the microscopic morphology of the resin poor area is shown.

intimate contact of the samples was measured with a novel method which considers the non-homogeneous nature of the contact surface. Experimental findings were compared to and contrasted with the state-of-the-art intimate contact models. In order to do that, a heat transfer model of the process was formulated to estimate the temperature history of the tape in the compaction region. The estimated temperature history was then combined with the measured roller pressure and the degree of intimate contact was calculated. The results were used to present a new approach to describe the intimate contact development during LAFP.

2. Materials and methods

2.1. Fiber placement system

Fiber placement experiments were conducted at Royal Netherlands Aerospace Center (NLR). A six-axis articulated robot on a linear axis provided by Coriolis was used. The machine was able to deliver eight 6.35 mm ($\frac{1}{4}$in.)-wide tapes simultaneously up to 800 mm/s placement speed. The end effector was equipped with a 6 kW Laserline LDF series diode laser system and an optic lens which created a 56 mm × 28 mm rectangular illuminated area at the 250 mm focal distance. A conformable compaction roller with 60 shore hardness and a diameter of 70 mm was installed on the machine. Fig. 3 depicts the fiber placement system used for this study.

2.2. Specimens for intimate contact investigation

The material used in this study was TC1320-1 CF/PEKK supplied by TenCate, in $\frac{1}{4}$ in. slit tapes. Eight tapes with cross-sectional dimensions 6.35mm × 0.15 mm were placed next to each other simultaneously along 1000 mm long strips on a flat aluminum tool with each combination of process parameters shown in Table 1. The machine parameters were chosen such that they cover the range between the minimum and maximum compaction forces and placement speeds relevant to the industrial use of LAFP at processing temperatures suggested by the manufacturer [29]. The temperature of the heated tool was set to 155 °C to allow the compacted tape to cool down to below its glass transition temperature (159 °C [29]), so that the amorphous phase of the PEKK polymer stays in the glassy state and does not cause further changes in the microstructure after compaction. The tool surface was covered with 50 μm thick polyimide (thermalimide) film to reduce the possible effects of the scratches on the tool on the degree of intimate contact measurements. Samples were cut from the mid-section (between 400 and 600 mm from the beginning) of the strips so that the acceleration and deceleration phases of the placement head did not affect the microstructure.

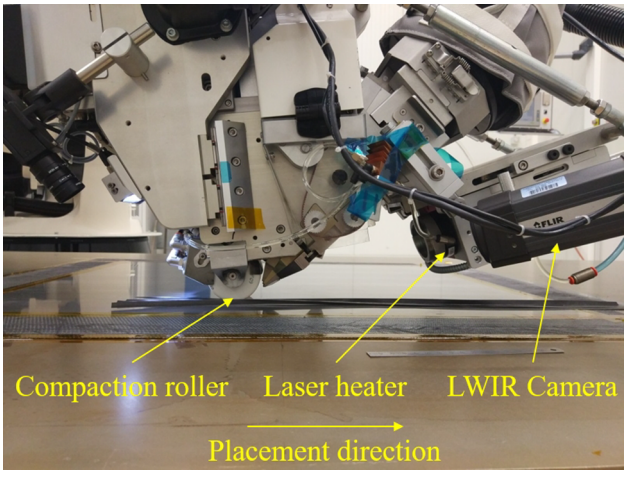

Fig. 3. The fiber placement system used in the experiments. Courtesy of Royal Netherlands Aerospace Center (NLR). (For interpretation of the references to color in this figure legend, the reader is referred to the web version of this article.)

Table 1
Process parameters used in the experimental study. A sample with each combination of parameters was manufactured.

Nip Point Temperature (°C)	Tool Temperature (°C)	Compaction Force (N)	Placement Speed (mm/s)
380	20	100	100
400	155	400	200
		800	400
			800

2.3. Process temperature measurement

The surface temperature of the visible nip point of the tape was measured using a long wave infrared (LWIR) camera. The apparent emissivity of the material is required for measuring the temperature with this method. To determine the apparent emissivity, a single layer of material was placed on the tool surface and a thermocouple was attached on the material surface. The material was heated by heating the tool and sufficient time was given to reach the steady state in the material. The end effector of the tape placement robot was positioned such that the thermal image was similar to actual placement conditions. Thermocouple readings were compared with thermal image readings of the same location. The calibration was performed around 220 °C and the apparent emissivity was found to be 0.85 for the CF/PEKK material.

2.4. Pressure measurement

Although the process is controlled by the so called “compaction force”, the actual pressure distribution under the compaction roller is unknown. During placement, the compaction roller applies the pressure while rotating. However, the effect of roller rotation on the normal pressure is negligible and the dynamic case can be simplified into a static one [33]. Fujifilm Prescale LLW pressure sensitive films were used to measure the contact area under the compaction roller. Pieces of the pressure sensitive film were fixed on the tool and different compaction forces were applied with the placement robot statically, as demonstrated in Fig. 4. A force range of 100 to 800 N was covered with steps of 100 N. Then, the dimensions of the stains on the pressure films were measured. It was assumed that the pressure distribution was uniform and the applied force was divided by the measured area to calculate the average compaction pressure.

3. Effective intimate contact

The resin-rich area on the surface is a pre-requisite for bond strength development between the subsequent layers, which is explained with the autohesion theory [7]. Therefore, the degree of intimate contact is meaningful only if it consists of resin-rich areas. However, current intimate contact models assume that the surface asperities are homogeneous. Considering the fiber-rich nature of the tape surface prior to compaction, there is a need for a new definition of the intimate contact phenomenon. Within a region of interest, the ratio of the compacted *resin-rich* area to the whole projected area is designated as the *degree of effective intimate contact* (DEIC) in this work.

3.1. Characterization

The methodology to obtain the degree of effective intimate contact is summarized in Fig. 5. Micrographs were taken from the tool side of the surfaces with a Keyence VHX-2000 system equipped with a VH-

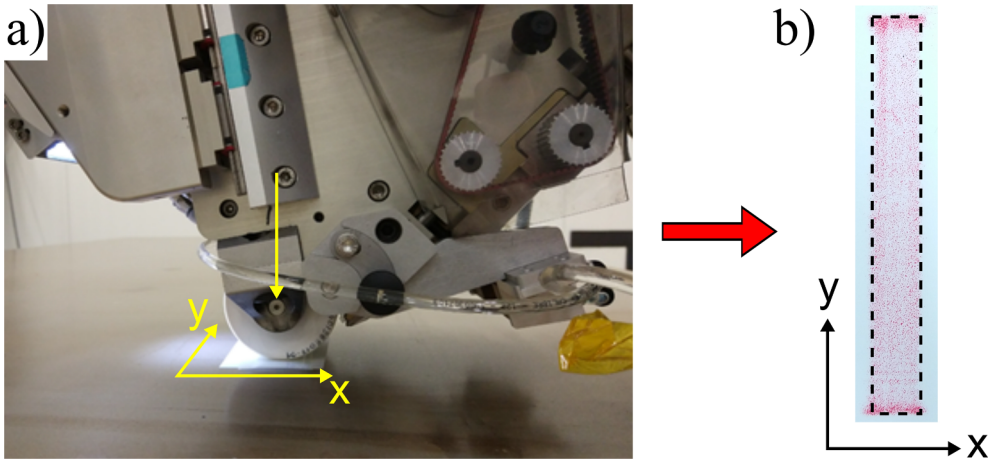

Fig. 4. (a) Static pressure application with the LAFP machine (b) a stained pressure film with the assumed uniform pressure area. (For interpretation of the references to color in this figure legend, the reader is referred to the web version of this article.)

Z100 lens. Five images were taken for each specimen with 200× magnification (image size approximately 1.6 × 1.2 mm^2). In the first step, grayscale intensity histograms were generated for each image using the software of the microscope. These histograms show how many pixels are present for each grayscale value in an interval of 0 and 255 where 0 is black and 255 is white. Peaks in such a histogram designates the clusters of pixels that belong to certain features in the image [34]. Two classes of histograms were observed. The first class of histograms belonged to the samples which have significant amount of resin-rich area on the surface after compaction. There were two clear peaks which represent the dry fibers (the peak with a lower greyscale value) and the compacted resin area (the peak with a higher grayscale value). For each image, a threshold was determined at the local minimum between the two peaks. The pixels with a grayscale value higher than this threshold were selected as the area in effective intimate contact. The second class of histograms were observed for the samples with a low amount of resin on the surface after compaction. Only a single peak was present in these histograms, making it difficult to set a threshold value. In such cases, the threshold was determined based on the point where the slope of the histogram curve is the closest to zero after the first peak as the grayscale intensity value increases. For both cases, this selected area included a low amount of dry fibers in addition to the compacted resin-rich areas. In an attempt to eliminate the dry fibers from the selected area, all sub-areas smaller than 500 μm^2 were excluded. This value was found to be appropriate for selecting the resin-rich areas as a result of trials with different minimum area thresholds on many images.

Two reference cases, unprocessed and fully compacted tapes, were examined with the proposed methodology to demonstrate its validity on the extreme cases and compare with the available intimate contact models. Fully compacted samples were created by compacting a single layer of a 30 mm × 30 mm of the same material in a press at a temperature of 380 °C and a pressure of 2 MPa for 20 min. These

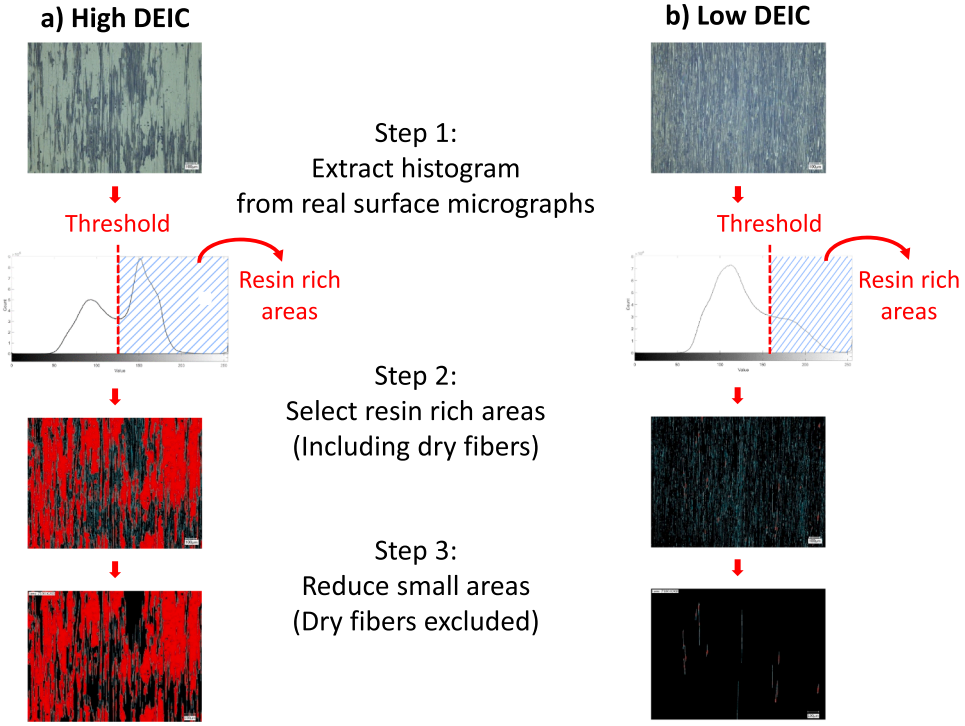

Fig. 5. Measurement of degree of effective intimate contact from histograms of optical microscope images. (For interpretation of the references to color in this figure legend, the reader is referred to the web version of this article.)

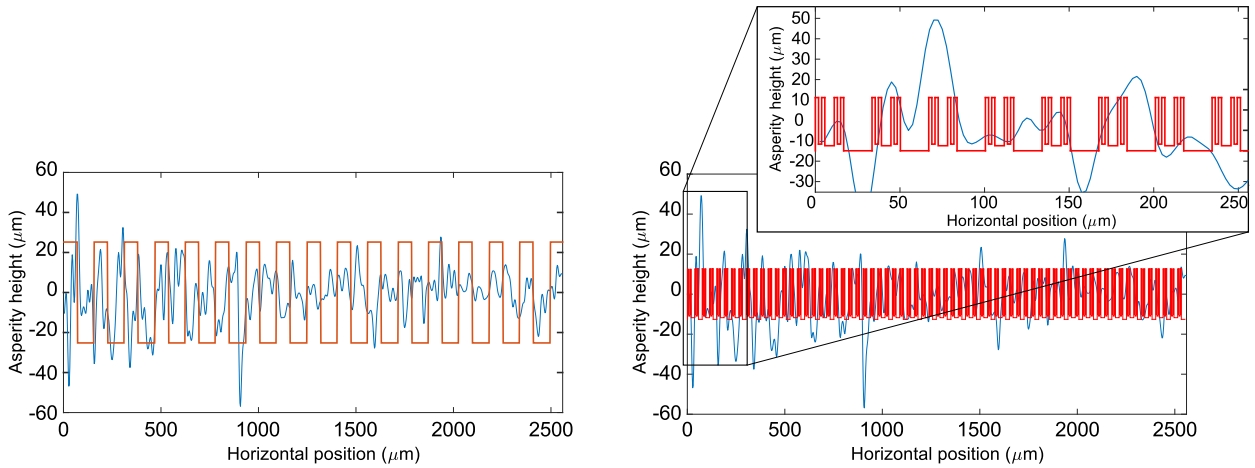

Fig. 6. Corresponding idealized surface representations on a real surface profile. (a) Uniform rectangle approximation and (b) Cantor set approximation (only first three generations are shown for clarity). (For interpretation of the references to color in this figure legend, the reader is referred to the web version of this article.)

parameters were determined based on prior experience with CF/PEKK materials.

Microstructure of the LAFP-processed strips were qualitatively investigated with cross-sectional microscopy for more insight about effective intimate contact development. Samples were embedded in epoxy and polished for this purpose. The same microscopy system is used to obtain the images.

3.2. ANOVA analysis

The analysis of variance (ANOVA) method was used to evaluate the effects of the process parameters given in Table 1 on the mean of the degree of effective intimate contact measurements. Matlab function *anovan* was used for this purpose [35]. The outputs of this function were p-values for each process parameter. p-values smaller than 0.05 imply that the mean response of the specific parameter is different from the mean of all data within a confidence interval of 95%. The effects of such a parameter can be considered statistically significant.

3.3. Intimate contact calculation based on squeeze flow models

Effective intimate contact measurements were compared with the squeeze flow-based intimate contact models. As explained in the following section, the temperature and pressure history of the material are required to calculate the final degree of intimate contact. The temperature history of the tape during compaction was calculated with a heat transfer model. The compaction pressure during the process was determined using the methodology presented in Section 2.4. These two process-induced parameters were then fed into two intimate contact models available in the literature.

3.3.1. Intimate contact models

Two squeeze flow-based intimate contact models were used to predict intimate contact development on a single tape processed with LAFP. The first model proposed by Lee and Springer [20] approximates the surface of the tape as a series of uniform rectangles. The degree of intimate contact can be found with the following equation:

$$D_{ic}(t) = \frac{1}{1+\frac{w_0}{b_0}}\left[1+5\left(1+\frac{w_0}{b_0}\right)\left(\frac{a_0}{b_0}\right)^2\int_0^{t_c}\frac{P_{app}}{\mu(T)}\mathrm{d}t\right]^{\frac{1}{5}} \tag{1}$$

where $\frac{w_0}{b_0}$ and $\frac{a_0}{b_0}$ are geometrical parameters defining the uniform rectangular representation, T is the temperature, P_{app} is the compaction pressure, t is the compaction time and $\mu(T)$ is the temperature dependent viscosity of the material. The geometrical parameters were obtained from real surface measurements with a procedure similar to the work of Schaefer et al. [32]. Surface profiles were measured with an Olympus LEXT OLS3100 confocal laser scanning microscope. The parameters $\frac{w_0}{b_0}$ and $\frac{a_0}{b_0}$ were found by calculating the average of the ratio of the material and gaps at different height levels within $\pm 2\sigma$ from the mean surface height, where σ designates the standard deviation.

The second model proposed by Yang and Pitchumani [22] approximates the composite surface as a fractal Cantor set and calculates the degree of intimate contact as follows:

$$D_{ic}(t) = \frac{1}{f^n}\left[\frac{5}{4}\left(\frac{h_0}{L_0}\right)^2 f^{\frac{2nD}{2-D}+n+4}\int_{t_{(n+1)}}^{t}\frac{P_{app}}{\mu(T)}\mathrm{d}t+1\right]^{\frac{1}{5}} \quad \text{for} \quad t_{(n+1)} \leqslant t \leqslant t_{(n)} \tag{2}$$

where f is the fractal scaling factor, n is the generation number of the Cantor set, D is the fractal dimension and $\frac{h_0}{L_0}$ is the ratio of the height of the first generation asperities to the Cantor block length. These parameters were determined as described in the original paper from real surface profiles and their power spectra. The rest of the parameters are the same with Eq. (1).

Fig. 6 demonstrates the corresponding idealized surface

Table 2
Surface parameters used in the intimate contact models.

Surface model	Parameter	Explanation	Value
Lee and Springer [20]	w_0/b_0	Ratio of asperity width to gap width	1.11
	a_0/b_0	Ratio of asperity height to asperity width	0.57
Yang and Pitchumani [22]	f	Scaling factor	1.09
	D	Fractal dimension	1.63
	h_0/L_0	Ratio of first generation asperity height to Cantor block length	0.20
	n	Total number of generations	15

representations for both intimate contact models on an example measured surface profile. The average geometrical parameters used for the intimate contact models are summarized in Table 2.

T was calculated from the heat transfer model in Section 3.3.2. P_{app} was obtained from static contact measurements described in Section 2.4. t was calculated by dividing the contact length obtained from the pressure sensitive films by the placement speed. $\mu(T)$ for CF/PEKK material was adapted from [36]. It is expressed as the following relation:

$$\mu(T) = 4.362 \times 10^{7} e^{-0.0401(T-623)} \text{ Pa s} \tag{3}$$

3.3.2. Heat transfer model

A three dimensional Lagrangian finite element (FE) model of the placed tape and the tool with a moving placement head configuration, based on authors' previous work [37], was used to estimate the transient through-thickness temperature distribution during compaction. Abaqus 2017 finite element package was used to create and solve the model.

The model solves the energy equation to find the transient temperature distribution $T(t)$ within the bodies, assuming the internal heat generation is negligible:

$$\rho C_p \frac{\partial T}{\partial t} = \nabla(k \nabla T) \tag{4}$$

where ρ is the density, C_p is the specific heat and k is the conductivity of the material. Referring to Fig. 7, the following boundary conditions were applied:

The aluminum tool was assumed to have a fixed temperature T_{tool} due to its large thermal mass. The incoming tape was assumed to reach uniform through-thickness temperature $T_{tape}(0)$ at the visible nip point. Past the visible nip point, the tape cools down due to the contact with the compaction roller in the shadow and compaction zones (see Fig. 1). Following that, the ambient air cools down the tape at the top surface. The heat loss to the compaction roller and the ambient air after compaction were formulated as a moving convection boundary condition:

$$k \nabla T = -h(T - T_a) \tag{5}$$

where h is the convection coefficient and T_a is the ambient temperature. The convection coefficient for the roller, h_r, and for the air, h_a, were taken as 400 W/m^2 K [38] and 10 W/m^2 K[39], respectively. T_a was approximated as 50 °C for the roller [40] and 20 °C for the ambient air. The coordinates of the areas where the convection boundary condition is active were updated with an Abaqus FILM subroutine.

At the tape-tool interface, the heat transfer was modeled with a thermal contact:

$$q = C(T_{tape} - T_{tool}) \tag{6}$$

where q is the heat flux between the tape and the tool and C is the thermal contact conductance. C was updated based on the location of the moving nip point and it was implemented with an Abaqus GAPCON subroutine. At the regions in front of the nip point, no heat transfer was possible between the tape and the tool. To impose this condition without creating numerical problems, the thermal contact conductance was set to a very low value, namely 10^{-5} W/m^2 K. The thermal contact conductance was set to 10^{6} W/m^2 K past the nip point, assuming almost perfect heat transfer occurs at the interface between the tape and the tool.

The temperature history of the tape was calculated for the scenario where the highest intimate contact is expected (the lowest placement speed (v) and the highest visible nip point temperature ($T_{tape}(0)$), tool temperature (T_{tool}) and compaction force in Table 1). The roller contact length at the compaction zone, L_c, was determined from the contact length measurements described in Section 2.4. The contact length for a compaction force of 800 N was used since it was observed that this parameter did not affect the temperature history significantly. The length of the shadow, L_s, was estimated from the computer aided design (CAD) drawings of the end effector. The process related and geometric parameters used in the model are summarized in Table 3. Thermal material properties provided in Table 4 were used for the composite tape.

DC3D8 linear hexahedral heat transfer elements were used to mesh the tape and the tool. The tape was meshed with 10, 120 and 6 uniform elements in the thickness, length and width directions, respectively.

4. Results

4.1. Pressure measurement

The average compaction pressure has a nonlinear relationship with the applied compaction force, as seen in Fig. 8. The compaction roller deforms more as the compaction force increases, creating a larger contact area. Even though a larger contact area is favorable for better intimate contact development, it poses a limitation on reaching high pressure. Comparison of the applied compaction force and average pressure under the roller provides useful information for further discussions.

4.2. Surface and cross-sectional micrographs

Effective intimate contact measurements of unprocessed tapes and fully consolidated samples are summarized in Table 5 along with the predictions made with Eqs. (1) and (2). Reflecting the fiber-rich structure of the surface, the degree of effective intimate contact was very low for the unprocessed tow. On the contrary, press consolidated samples

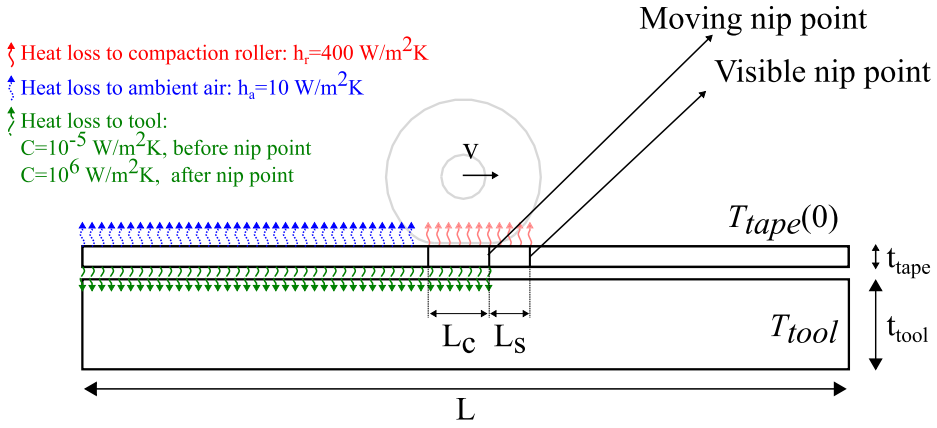

Fig. 7. Modeling space and moving boundary conditions in the FE model. h and C represent the applied convection coefficient and thermal conductance, respectively. For the other parameters, please refer to Table 3. (For interpretation of the references to color in this figure, the reader is referred to the web version of this article.).

Table 3
The process related and geometric parameters used in the heat transfer model.

Parameter	Symbol	Value	Unit
Tape temperature prior the visible nip point	$T_{tape}(0)$	400	°C
Fixed tool temperature	T_{tool}	155	°C
Placement speed	v	100	mm/s
Compaction pressure (for intimate contact models)	P_{app}	0.29–0.86	MPa
Roller contact length in the compaction zone	L_c	16	mm
Roller contact length in the shadow zone	L_s	4	mm
Domain length	L	100	mm
Tape thickness	t_{tape}	0.15	mm
Tool thickness	t_{tool}	30	mm
Tape width		50.8	mm

Table 4
Thermal material properties of CF/PEKK.

Density[a] (kg/m^3)	Thermal conductivity (W/m °C)		Specific Heat[d] (J/kg °C)	Temperature (°C)
	Longitudinal[b]	Transverse [c]		
1506	6	0.73	990	50
			1176	100
			1353	150
			1675	200
			1865	250
			2220	300
			2289	350

[a] Measured at room temperature according to ASTM D792.
[b] Estimated from [38], based on the similarity of transverse thermal conductivity to APC-2.
[c] Averaged from [50].
[d] Measured with differential scanning calorimetry with a heating rate of 20 °C/s.

showed almost complete effective intimate contact. The major difference between the predictions and measurements can be observed for the unprocessed tape. Both squeeze flow models indicate that the unprocessed tape is in considerable intimate contact with a hypothetical opposite surface, as demonstrated in Fig. 6. However, since the models consider only the surface profiles and not the microstructure, the effect of resin content at the surface is not accounted for. The effective intimate contact concept illustrated in Fig. 5 provides a methodology which is sensitive to the resin content at the surface and able to measure the whole range of degree of effective intimate contact (i. e., 0–100%) for the fiber-placed samples.

Table 5
Degree of effective intimate contact of the reference cases and degree of intimate contact predictions with the currently available models.

	Measured DEIC (%)	Lee & Springer (%)	Yang & Pitchumani (%)
Unprocessed Tape	0.2 ± 0.4	47.4	27.5
Press Consolidated Ply (at 380 °C, 20 min)	96.6 ± 1.8	100	100

The surface micrographs shown in Fig. 9 demonstrate the morphology of the contact surface for a range of effective intimate contact levels. In Fig. 9a, a specimen with a low degree of effective intimate contact (1%) is shown. The surface exhibits very low amounts of resin content and the surface is covered with dry fibers. In Fig. 9b, a surface with slightly higher amount of degree of intimate contact (23%) is shown. Squeezed out and flattened resin portions are apparent. Fibers are covered with this squeezed-out resin locally. Flattened resin regions mostly elongate along fibers since dry fibers restrict the motion of the molten resin more in the perpendicular direction. The micrograph in Fig. 9c shows a high degree of effective intimate contact obtained within this study (57%), where more resin is squeezed out and covers a larger portion of the surface. The constraining effect of the dry fibers can still be observed on the wetting behavior of the resin material. Within large impregnated areas, some gaps elongated in the fiber direction exist.

Representative cross-sectional micrographs of specimens manufactured with the same nip point temperature (400 °C) and placement speed (100 mm/s) but different compaction forces (100N and 800N) are shown in Fig. 10. Such a comparison is informative about the change in the microstructure during the intimate contact development. Fig. 10a shows a sample with low intimate contact development (22.2%) due to low compaction force. In addition to flattened fiber-resin mixture, incompletely compacted (non-flat) resin-fiber mixture and loose dry fibers can be observed at the surface on the tool side. The specimen in Fig. 10b represents a specimen with higher degree of intimate contact (54.8%) since higher compaction force results in more deformation at the surface given the same thermal history (Eqs. (1) and (2)). Regions with resin-fiber mixture at the surface on the tool side are mostly flattened. Dry fibers are present; however, it can be observed that they are compressed more than the case with the lower compaction force.

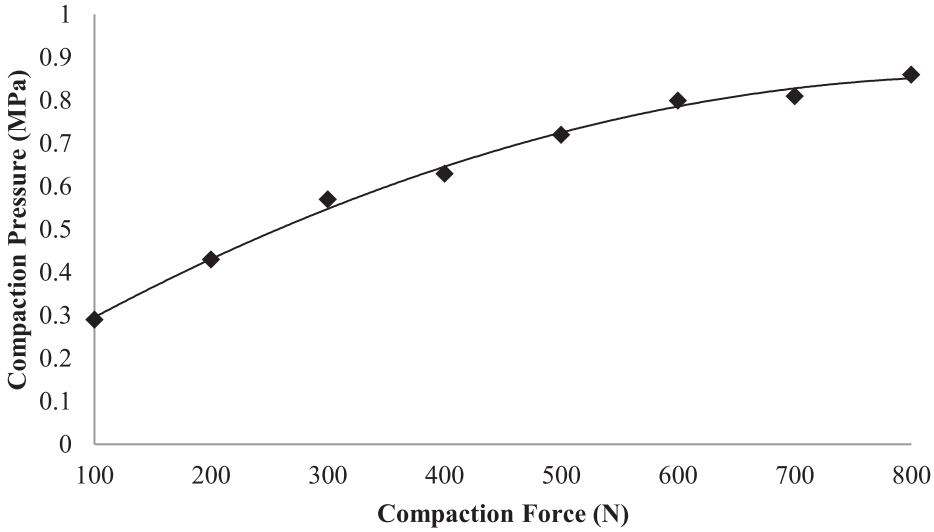

Fig. 8. Nonlinear relation between the applied compaction force and the average compaction pressure measured with pressure sensitive films due to the increasing contact area.

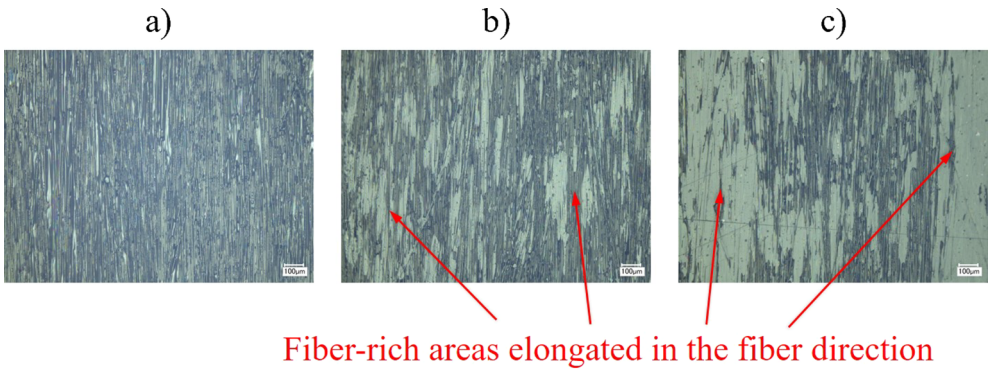

Fig. 9. Representative surface micrographs for different levels of effective intimate contact: (a) 1% (T_{tool} = 20 °C, T_{np} = 380 °C, F = 100 N, V = 100mm/s), (b) 23% (T_{tool} = 155 °C, T_{np} = 400 °C, F = 400 N, V = 400mm/s), (c) 57% (T_{tool} = 155 °C, T_{np} = 400 °C, F = 800 N, V = 400 mm/s). (For interpretation of the references to color in this figure legend, the reader is referred to the web version of this article.)

4.3. Effects of process parameters on intimate contact development

Final degrees of effective intimate contact at different tool temperatures, nip point temperatures, compaction forces and placement speeds are summarized in Fig. 11. ANOVA analysis is applied on this data set to find statistically significant parameters on effective intimate contact development.

4.3.1. ANOVA analysis

The results presented in Table 6 indicate that the sources tool temperature (TT), compaction force (CF), placement speed (PS) and the interaction terms TT∗CF and TT∗PS caused statistically significant differences on the degree of effective intimate contact within the parameters presented in Table 1. For the other sources, it is not possible to distinguish the effects from experimental scatter. Significance of the interaction terms (sources TT∗CF and TT∗PS) shows that the effect of the tool temperature dominates over the others. This is also evident in Fig. 11: samples placed on the cold tool (top row) have very low degrees of effective intimate contact compared to the samples placed on the hot tool (bottom row) and effects of compaction force and placement speed are not apparent. Therefore, in order to assess the effects of compaction force and placement speed, the results from the hot tool should be used.

Interestingly, the target nip point temperature (source NPT) did not cause significant changes on the degree of effective intimate contact. Although the squeeze flow viscosity of CF/PEKK decreases more than twice when the temperature increases from 380 °C to 390 °C according to Eq. (3), this decrease was not reflected in the results as an increase in effective intimate contact development. A possible explanation is the very short time spent above the melting temperature due to the quenching effect of the tool. Hence, data from two different nip point temperatures were combined to present the results of the effects of compaction force and placement speed.

4.3.2. Compaction force

The effect of the compaction force on the degree of effective intimate contact is shown in Fig. 12. The horizontal axis of the figure is replaced with the compaction pressure instead of the compaction force, according to the relationship presented in Fig. 8. The compaction forces of 100, 400 and 800 N correspond to the average compaction pressures of 0.29, 0.63 and 0.86 MPa, respectively. A linear fit can express the relationship for every placement speed. It should be noted that the linear relationship holds true only for the compaction pressure under the roller instead of the applied compaction force. As the placement speed increases, the effect of the compaction pressure decreases, which is shown with a decrease in the slope of the fit curves.

4.3.3. Placement speed

The effect of the placement speed on the degree of effective intimate contact is shown in Fig. 13. As the process speed increases, the time available for compaction decreases. A non-linear decrease is observed as the placement speed increases. At the lowest compaction force (100 N), the degree of effective intimate contact is affected less by the increasing placement speed and no significant change was observed above 100 mm/s.

4.4. Temperature history and intimate contact predictions

The calculated temperature history of the top and bottom sides of the tape are shown in Fig. 14. In the non-illuminated shadow zone, the temperature of the tape decreases unevenly in the thickness direction until it reaches the nip point (the beginning of the consolidation zone). The top surface of the tape cools down faster than the bottom side due to direct contact with the roller. When the tape reaches the nip point, the bottom and top surfaces are at 383 °C and 375 °C, respectively. However, as soon as the tape enters the consolidation zone, the bottom surface of the tape quenches to the mold temperature rapidly (Fig. 14b). This causes the bottom surface to stay above the melting temperature for only 2.5 ms. On the other hand, the top surface stays above the melting temperature for 15 ms, a considerably longer duration.

The degree of intimate contact predictions based on the calculated temperature history of the bottom side of the tape are shown in Fig. 15 along with the experimental results. Similar trends were observed for the fractal and uniform rectangular intimate contact models. Despite the increase in pressure, almost no change occurs in the predictions. Due to the very limited time spent above the melting temperature at the bottom surface of the tape, the surface asperities do not flatten and the final degree of intimate contact calculation is dominated by the initial

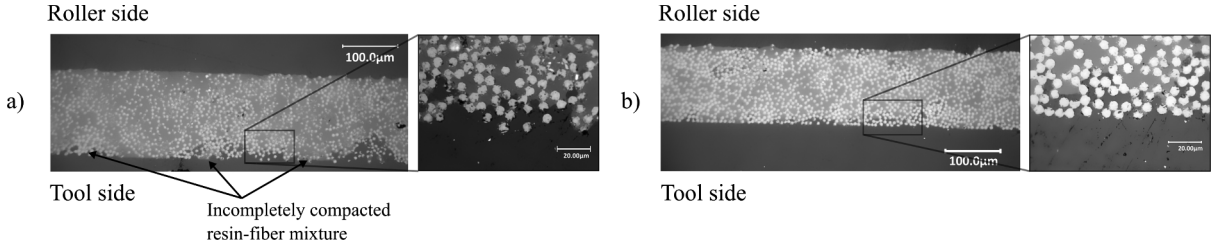

Fig. 10. Representative cross-section micrographs for different levels of compaction force at the same nip point temperature (400 °C) and process speed (100mm/s). (a) 100 N, loose dry fibers in magnified view. (b) 800 N, compressed dry fibers in magnified view.

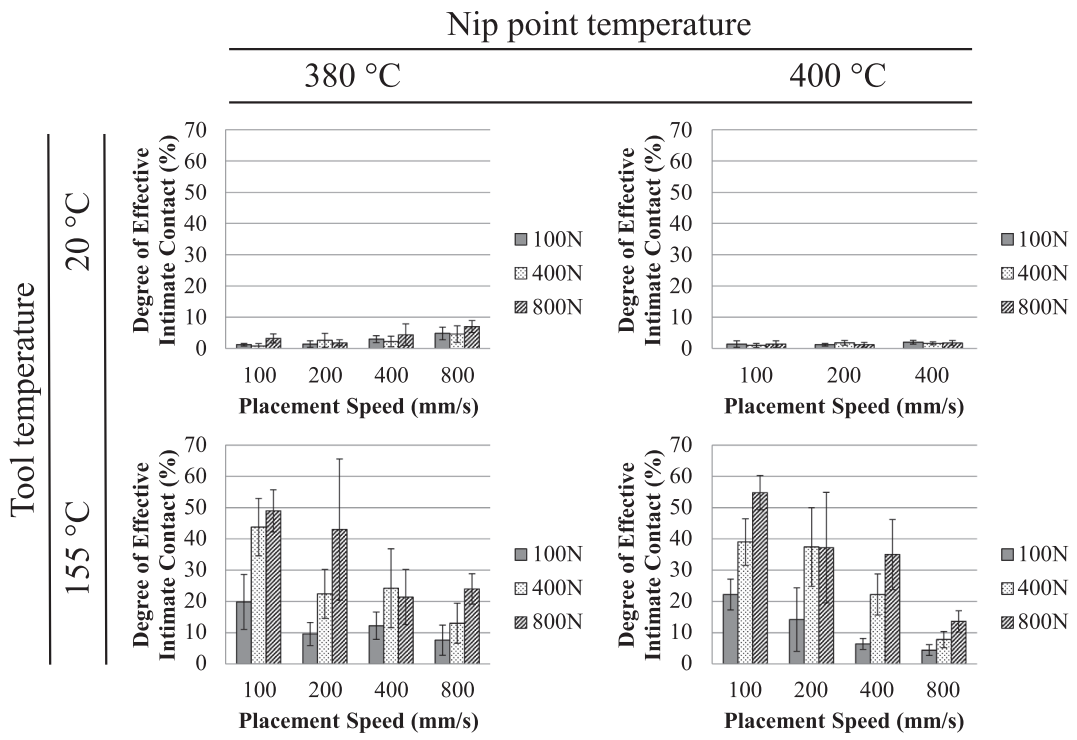

Fig. 11. Experimental degree of effective intimate contact for all process parameters. Top row: cold tool (20 °C), bottom row: hot tool (155 °C), left column: 380 °C nip point temperature, right column: 400 °C nip point temperature. The error bars show the standard deviation.

Table 6
Results of the multiway ANOVA. Asterisk symbol (∗) designates the interaction between the related parameters. $p < 0.05$ means that the effect of the parameter or the interaction is statistically significant.

Source	p-value
Tool temperature (TT)	0
Compaction force (CF)	0
Placement speed (PS)	0
Nip point temperature (NPT)	0.3684
TT∗CF	0
TT∗PS	0
TT∗NPT	0.2586
CF∗PS	0.3065
CF∗NPT	0.956
PS∗NPT	0.2065

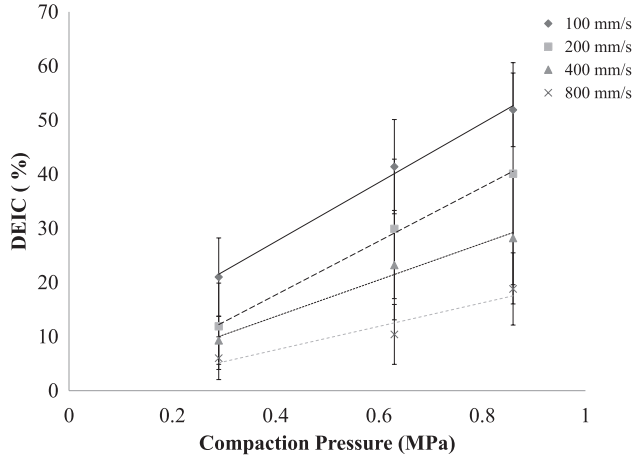

Fig. 12. Degree of effective intimate contact as a function of the average compaction pressure under the roller at different placement speeds.

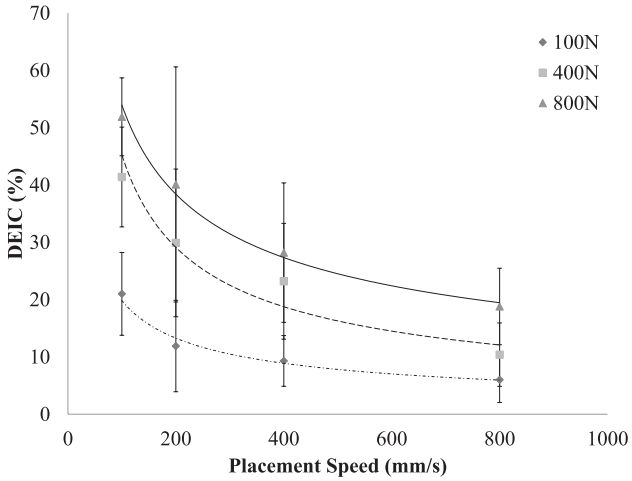

Fig. 13. Degree of effective intimate contact as a function of placement speed at different compaction forces.

surface parameters given in Table 2. The results are, therefore, only shown for the slowest placement speed (100mm/s) since the predictions for higher placement speeds would result in the same final degree of intimate contact.

5. Discussion

Based on the results of surface and cross-sectional microscopy, it can be stated that intimate contact development during LAFP is a combination of multiple mechanisms. Squeeze flow of surface asperities, the common approach to explain intimate contact development for thermoplastic composites [19,20,22], plays a partial role. As seen in Fig. 10, samples manufactured with lower compaction forces contain incompletely deformed surface asperities filled with a mixture of fiber and resin. As the material is processed with higher compaction forces,

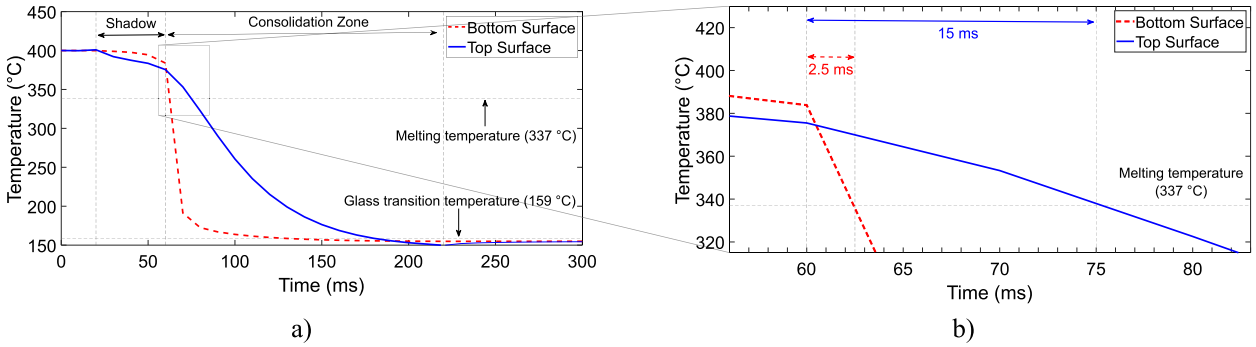

Fig. 14. Calculated temperature history of the thermoplastic tape. (a) Full history. (b) Magnified view of consolidation zone above the melting temperature. Time spent above the melting temperature under the compaction roller is designated with a blue arrow for the top surface and a dashed red arrow for the bottom surface. (For interpretation of the references to color in this figure legend, the reader is referred to the web version of this article.)

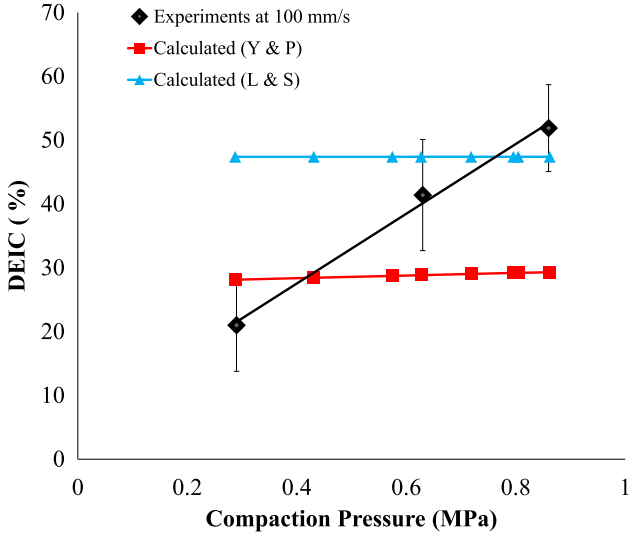

Fig. 15. Experimentally obtained degree of effective intimate contact and calculated intimate contact based on calculated thermal history. Placement speed: 100 mm/s. L & S: Uniform rectangular surface representation [20], Y & P: Fractal surface representation [22]. (For interpretation of the references to color in this figure legend, the reader is referred to the web version of this article.)

incompletely deformed surface asperities are less apparent. Clusters of dry fibers are present for all cases. At high compaction forces, although the squeeze flow of surface asperities seems to be completed, full effective intimate contact is not achieved. A portion of the compaction energy is spent on compressing the dry fiber clusters and does not result in effective intimate contact development.

Effective intimate contact development at the fiber-rich regions cannot be explained by the squeeze flow of a fiber-resin mixture. Resin infiltration, which has been investigated for other composite manufacturing methods [41,42], should be taken into consideration. Two mechanisms can be identified for impregnation of dry fiber bundles. The first mechanism is the through-thickness percolation flow of the resin. The resin needs to permeate towards the surface to facilitate effective intimate contact. The other mechanism is the in-plane flow of resin at the compaction surface. This mechanism is effective mostly in the fiber direction because the dry fiber network restricts the resin flow in the direction perpendicular to fibers. As a result, the fiber-rich areas within the impregnated zones are typically elongated in the fiber direction, as demonstrated in Fig. 9. This observation is in-line with the literature, where the permeability in the fiber direction is reported to be an order of magnitude higher than the permeability in the transverse direction [43,44]. Fig. 16 schematically depicts the proposed effective intimate contact development during LAFP based on our observations. In Fig. 16a, the state of the thermoplastic composite tape prior to the nip point is shown. Zones 1 and 3 are fiber-rich regions, whereas Zone 2 represents the resin-rich portions of the material. After compaction (Fig. 16b), all of these regions are in physical contact. However, Zone 1 is not in effective intimate contact since no resin is present at the interface. Zone 2 achieves effective intimate contact with the squeeze flow mechanism. Zone 3 requires through thickness and in-plane percolation flow to establish effective intimate contact.

The share of these separate mechanisms on effective intimate contact development depends on the initial fiber-resin distribution of the tape and severity of microstructural changes during the heating phase of LAFP. Initial fiber-resin distribution of a thermoplastic composite tape highly depends on the tape manufacturing processes. Although similar constituents and specifications are provided for tapes produced by different manufacturers, fiber uniformity, resin content at the surface and void size/distribution varies [45–47]. In connection with the initial state of the material, the heating phase affects tapes manufactured by different suppliers differently, as reported in [28]. Also, the state of the substrate at the nip point should be considered for an accurate analysis of the final degree of effective intimate contact at each interface in a fiber placed laminate, which is beyond the scope of this work. Therefore, more efforts should be spent on understanding the microstructure of the thermoplastic tape and substrate just before the nip point during LAFP.

The response of the experimentally obtained degree of effective intimate contact to increasing compaction pressure differed from the response of the degree of intimate contact predicted by Eqs. (1) and (2), which use the squeeze flow assumptions. Intimate contact development based on homogenized transverse squeeze flow models were not sensitive to an increase in pressure. This insensitivity can be explained by the fact that only the surface temperature was used for predicting intimate contact development with the squeeze flow models. With the quenching effect of the tool surface, the resin near the surface is expected to cool down rapidly. However, molten resin is present through the thickness of the tape for a longer duration and contributes to the effective intimate contact development via percolation flow. Such a mechanism can also explain bonding below melting temperature, reported for CF/PPS tapes welded onto carbon woven fabric reinforced PPS laminates [48] and CF/PEEK laminates manufactured with LAFP [27]. This phenomenon was attributed to the autohesion of the amorphous chains in the semi-crystalline polymer at temperatures between the melting and glass transition temperatures. However, bonding was found to be limited to the intimate contact development in both works, indicating that its effect on the inter-laminar bond development was more pronounced than the autohesion mechanism. This means that the effective intimate contact development concept, which is introduced in this paper, might improve the accuracy of bonding predictions.

The samples manufactured with different placement speeds at a

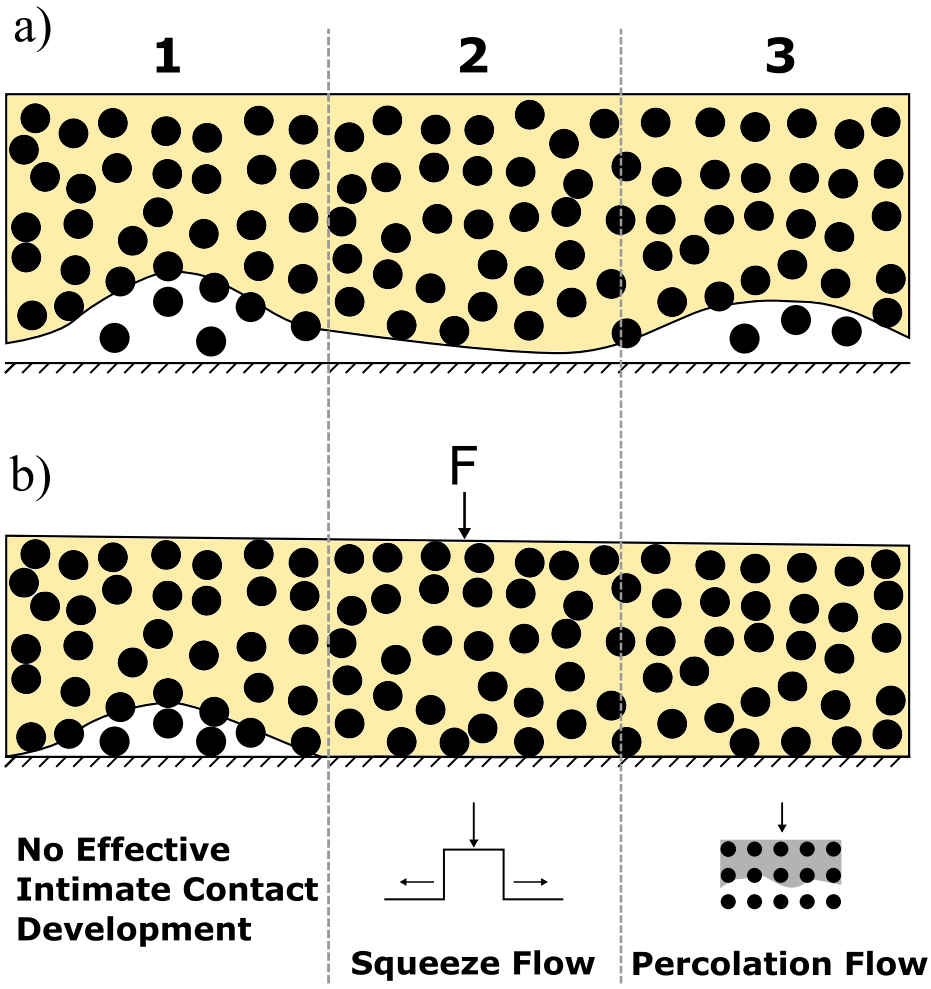

Fig. 16. Development of effective intimate contact and underlying mechanisms for initial surfaces with different microstructure. (a) Uncompressed composite tape, (b) compressed composite tape. (For interpretation of the references to color in this figure legend, the reader is referred to the web version of this article.)

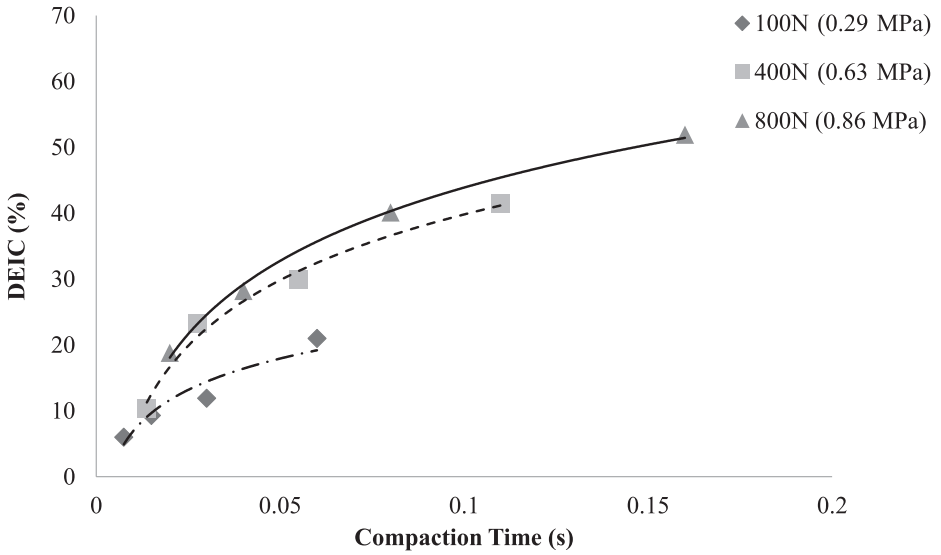

Fig. 17. Time dependent effective intimate contact development based on different placement speeds at constant compaction force.

fixed compaction force can be linked to different stages of intimate contact development. Fig. 17 shows effective intimate contact development as a function of compaction time, calculated by dividing the contact length obtained from pressure sensitive films by the placement speed. Experimental data for intimate contact development available in the literature covers a range from tens to hundreds of seconds [19,20,22]. Since only a fraction of a second is available for compaction during LAFP, it is difficult to make a direct comparison. However, the

trends show resemblance in terms of a steep increase at the beginning of compaction, followed by a decrease in the evolution rate. The same behavior was also confirmed for small time scales by numerical calculations presented in [49]. Two reasons can be identified as the reason for this behavior. The first one is the squeeze flow mechanism, which occurs at the resin-rich regions of the surface. Initially, the surface asperities have less contact and high local pressure, causing a rapid increase in the degree of effective intimate contact. As the asperities deform, increased contact area decreases the local pressure. Therefore, the evolution of the degree of effective intimate contact slows down. The second mechanism is the cooling of the tape as demonstrated in Fig. 14. The drop in temperature plays a hindering role for both the squeeze flow and percolation flow mechanisms as it causes the polymer viscosity to increase.

6. Conclusion

Intimate contact development during LAFP is a complex process involving multiple mechanisms. Due to short compaction times and very limited time available above the melting temperature of the semi-crystalline polymer, complete resin flow cannot be established at the tape surface as in conventional processing methods such as press molding and autoclave. Dry fibers were observed at the material surface after compaction, meaning that complete mechanical contact with the opposing surface might not contribute to the elimination of the inter-laminar voids or development of bonding strength. In order to quantify the amount of flattened resin content at the surface, the concept of *effective intimate contact* was proposed and a methodology to obtain the degree of effective intimate contact from surface micrographs was presented.

Effective intimate contact develops with squeeze flow at the resin-rich portions of the surface; however, through-thickness and in-plane percolation flow is required to impregnate the regions with compressed dry fibers. Due to the percolation flow mechanism playing a role, the through-thickness temperature distribution of the tape gains importance for effective intimate contact development during the LAFP process. Currently available intimate contact models could not predict the experimentally obtained degree of effective intimate contact since they consider the material surface as a homogeneous fiber-resin mixture which deforms only with the squeeze flow mechanism. In addition, the through-thickness temperature distribution was not accounted for. Future work is identified as modeling effective intimate contact development with all contributing mechanisms and performing experiments for model validation.

CRediT authorship contribution statement

Ozan Çelik: Conceptualization, Methodology, Software, Formal analysis, Investigation, Visualization, Writing - original draft, Writing - review & editing. **Daniël Peeters:** Conceptualization, Writing - review & editing, Supervision. **Clemens Dransfeld:** Conceptualization, Writing - review & editing, Supervision. **Julie Teuwen:** Conceptualization, Methodology, Writing - review & editing, Supervision.

Acknowledgments

This work is funded by European Regional Development Fund (ERDF) within the Smart Industry Fieldlab: ACM project under Grant No. KVW-00043. The authors would also like to thank Royal Netherlands Aerospace Center (NLR), especially Chris Groenendijk and Michiel Mandemaker, for the assistance with the LAFP machine.

References

[1] Beyeler EP, Phillips W, Guceri SI. Experimental investigation of laser-assisted thermoplastic tape consolidation. J Thermoplast Compos Mater 1988;1(1):107–21. https://doi.org/10.1177/089270578800100109.
[2] Choe CR, Lee KH. Nonisothermal crystallization kinetics of poly(etheretherketone) (PEEK). Polym Eng Sci 1989;29(12):801–5. https://doi.org/10.1002/pen.760291208.
[3] Roux M, Eguémann N, Dransfeld C, Thiébaud F, Perreux D. Thermoplastic carbon fibre-reinforced polymer recycling with electrodynamical fragmentation: from cradle to cradle. J Thermoplast Compos Mater 2017;30(3):381–403. https://doi.org/10.1177/0892705715599431.
[4] Grant C. Automated processes for composite aircraft structure. Industr Robot 2006;33(2):117–21. https://doi.org/10.1108/01439910610651428.
[5] Pitchumani R, Ranganathan S, Don RC, Gillespie JW, Lamontia MA. Analysis of transport phenomena governing interfacial bonding and void dynamics during thermoplastic tow-placement. Int J Heat Mass Transf 1996;39(9):1883–97. https://doi.org/10.1016/0017-9310(95)00271-5.
[6] Sonmez FO, Hahn HT. Analysis of the on-line consolidation process in thermoplastic composite tape placement. J Thermoplast Compos Mater 1997;10:543–72.
[7] Yang F, Pitchumani R. Nonisothermal healing and interlaminar bond strength evolution during thermoplastic matrix composites processing. Polym Compos 2003;24(2):263–78. https://doi.org/10.1002/pc.10027.
[8] Tierney J, Gillespie JW. Crystallization kinetics behavior of PEEK based composites exposed to high heating and cooling rates. Compos Part A: Appl Sci Manuf 2004;35(5):547–58. https://doi.org/10.1016/j.compositesa.2003.12.004.
[9] Grouve WJB, Warnet LL, Rietman B, Akkerman R. On the weld strength of in situ tape placed reinforcements on weave reinforced structures. Compos Part A: Appl Sci Manuf 2012;43(9):1530–6. https://doi.org/10.1016/j.compositesa.2012.04.010.
[10] Barasinski A, Leygue A, Soccard E, Poitou A. Identification of non uniform thermal contact resistance in automated tape placement process. Int J Mater Form 2014;7(4):479–86. https://doi.org/10.1007/s12289-013-1144-9.
[11] Simacek P, Advani SG, Gruber MB, Jensen B. A non-local void filling model to describe its dynamics during processing thermoplastic composites. Compos Part A: Appl Sci Manuf 2013;46(1):154–65. https://doi.org/10.1016/j.compositesa.2012.10.015.
[12] Comer AJ, Ray D, Obande WO, Jones D, Lyons J, Rosca I, et al. Mechanical characterisation of carbon fibre-PEEK manufactured by laser-assisted automated-tape-placement and autoclave. Compos Part A: Appl Sci Manuf 2015;69:10–20. https://doi.org/10.1016/j.compositesa.2014.10.003.
[13] Stokes-Griffin CM, Compston P. The effect of processing temperature and placement rate on the short beam strength of carbon fibre-PEEK manufactured using a laser tape placement process. Compos Part A: Appl Sci Manuf 2015;78:274–83. https://doi.org/10.1016/j.compositesa.2015.08.008.
[14] Weiler T, Emonts M, Wollenburg L, Janssen H. Transient thermal analysis of laser-assisted thermoplastic tape placement at high process speeds by use of analytical solutions. J Thermoplast Compos Mater 2018;31(3):311–38. https://doi.org/10.1177/0892705717697780.
[15] Kim YH, Wool RP. A theory of healing at a polymer-polymer interface. Macromolecules 1983;16(7):1115–20. https://doi.org/10.1021/ma00241a013.
[16] Butler CA, McCullough RL. An analysis of mechanisms governing fusion bonding of thermoplastic composites. J Thermoplast Compos Mater 1998;11:339–63. https://doi.org/10.1177/089270579801100404.
[17] Mehdikhani M, Gorbatikh L, Verpoest I, Lomov SV. Voids in fiber-reinforced polymer composites: a review on their formation, characteristics, and effects on mechanical performance. J Compos Mater 2019;53(12):1579–669. https://doi.org/10.1177/0021998318772152.
[18] Levy A, Heider D, Tierney J, Gillespie JW. Inter-layer thermal contact resistance evolution with the degree of intimate contact in the processing of thermoplastic composite laminates. J Compos Mater 2014;48(4):491–503. https://doi.org/10.1177/0021998313476318.
[19] Dara PH, Loos AC. Thermoplastic matrix composite processing model. Tech. Rep. Virginia: NASA; 1985.
[20] Lee WI, Springer GS. A model of the manufacturing process of thermoplastic matrix composites. J Compos Mater 1987;21(11):1017–55. https://doi.org/10.1177/002199838702101103.
[21] Mantell SC, Springer GS. Manufacturing process models for thermoplastic composites. J Compos Mater 1992;26(16):2348–77. https://doi.org/10.1177/002199839202601602.
[22] Yang F, Pitchumani R. A fractal Cantor set based description of interlaminar contact evolution during thermoplastic composites processing. J Mater Sci 2001;36(19):4661–71. https://doi.org/10.1023/A:1017950215945.
[23] Mantell SC, Wang Q, Springer GS. Processing thermoplastic composites in a press and by tape laying-experimental results. J Compos Mater 1992;26:2378–401. https://doi.org/10.1177/002199839202601603.
[24] Tierney J, Gillespie JW. Modeling of in situ strength development for the thermoplastic composite tow placement process. J Compos Mater 2006;40(16):1487–506. https://doi.org/10.1177/0021998306060162.
[25] Khan MA, Mitschang P, Schledjewski R. Parametric study on processing parameters and resulting part quality through thermoplastic tape placement process. J Compos Mater 2013;47(4):485–99. https://doi.org/10.1177/0021998312441810.
[26] Stokes-Griffin CM, Compston P. An inverse model for optimisation of laser heat flux distributions in an automated laser tape placement process for carbon-fibre/PEEK. Compos Part A: Appl Sci Manuf 2016;88:190–7. https://doi.org/10.1016/j.compositesa.2016.05.034.
[27] Stokes-Griffin CM, Compston P. Investigation of sub-melt temperature bonding of carbon-fibre/PEEK in an automated laser tape placement process. Compos Part A: Appl Sci Manuf 2016;84:17–25. https://doi.org/10.1016/j.compositesa.2015.12.019.
[28] Kok T. On the consolidation quality in laser assisted fiber placement: the role of the

heating phase. [Phd thesis]. University of Twente; 2018. https://doi.org/10.3990/1.9789036546065.
[29] TenCate Cetex® TC1320 PEKK Resin System Product Data Sheet; 2015.
[30] TenCate Cetex® TC1200 PEEK Resin System Product Data Sheet; 2017.
[31] Kok T, Grouve WJB, Warnet LL, Akkerman R. Intimate contact development in laser assisted fiber placement. ECCM17 - 17th European conference on composite materials. 2016. p. 26–30. 1(June).
[32] Schaefer PM, Guglhoer T, Sause MG, Drechsler K. Development of intimate contact during processing of carbon fiber reinforced Polyamide-6 tapes. J Reinf Plast Compos 2017;36(8):593–607. https://doi.org/10.1177/0731684416687041.
[33] Jiang J, He Y, Ke Y. Pressure distribution for automated fiber placement and design optimization of compaction rollers. J Reinf Plast Compos 2019. https://doi.org/10.1177/0731684419850896.
[34] Burger W, Burge MJ. Principles of digital image processing: advanced methods. Undergraduate Topics in Computer Science. London: Springer; 2013. doi: 10.1007/978-1-84882-919-0.
[35] The MathWorks Inc,. MATLAB and Statistics Toolbox Release 2017b; 2017.
[36] Lin HR, Advani SG. Processing models and characterization of thermoplastic composite wound parts. Polym Compos 1997;18(3):405–11. https://doi.org/10.1002/Pc.10291.
[37] Çelik O, Shroff S, Teuwen JJE, Bergsma OK, Benedictus R. A 3-D finite element model for thermal analysis of laser assisted fiber placement. SAMPE Europe. Southampton. 2018.
[38] Sonmez FO, Hahn HT. Modeling of heat transfer and crystallization in thermoplastic composite tape placement process. J Thermoplast Compos Mater 1997;10(3):198–240. https://doi.org/10.1177/089270579701000301.
[39] Cogswell FN. Thermoplastic aromatic polymer composites: a study of the structure, processing, and properties of carbon fibre reinforced polyetheretherketone and related materials. Butterworth-Heinemann; 1992. https://doi.org/10.1016/B978-0-7506-1086-5.50002-1.
[40] Stokes-Griffin CM, Compston P. A combined optical-thermal model for near-infrared laser heating of thermoplastic composites in an automated tape placement process. Compos Part A: Appl Sci Manuf 2015;75:104–15. https://doi.org/10.1016/j.compositesa.2014.08.006.
[41] Sommer JL, Mortensen A. Forced unidirectional infiltration of deformable porous media. J Fluid Mech 1996;311(1):193–217. https://doi.org/10.1017/S002211209600256X.
[42] Michaud V, Törnqvist R, Månson JA. Impregnation of compressible fiber mats with a thermoplastic resin. Part II: experiments. J Compos Mater 2001;35(13):1174–200. https://doi.org/10.1106/MLLN-4EF9-4KFU-XCWL.
[43] Gebart BR. Permeability of unidirectional reinforcements for RTM. J Compos Mater 1992;26(8):1100–33. https://doi.org/10.1177/002199839202600802.
[44] Zarandi MAF, Arroyo S, Pillai KM. Longitudinal and transverse flows in fiber tows: evaluation of theoretical permeability models through numerical predictions and experimental measurements. Compos Part A: Appl Sci Manuf 2019;119:73–87. https://doi.org/10.1016/j.compositesa.2018.12.032.
[45] Lamontia, M.A., Gruber, M.B. Remaining developments required for commercializing in situ thermoplastic ATP. In: Proceedings of the SAMPE 2007 Conference. Baltimore, MD. p. 1–15, ISBN 1934551007; 2007.
[46] Gruber MB, Lockwood I, Dolan T, Funck S, Tierney J, Simacek P, et al. Thermoplastic in situ placement requires better impregnated tapes and tows. In: International SAMPE technical conference; 2012. p. 1–15, ISBN 9781934551127.
[47] Slange TK, Warnet LL, Grouve WJB, Akkerman R. Influence of prepreg characteristics on stamp consolidation. AIP Conf Proc 2017;1896:30032. https://doi.org/10.1063/1.5008021.
[48] Grouve WJB, Warnet LL, Rietman B, Visser HA, Akkerman R. Optimization of the tape placement process parameters for carbon-PPS composites. Compos Part A: Appl Sci Manuf 2013;50:44–53. https://doi.org/10.1016/j.compositesa.2013.03.003.
[49] Leon A, Argerich C, Barasinski A, Soccard E, Chinesta F. Effects of material and process parameters on in-situ consolidation. Int J Mater Form 2019;12(4):491–503. https://doi.org/10.1007/s12289-018-1430-7.
[50] Coulson M, Dantras E, Olivier P, Gleizes N, Lacabanne C. Thermal conductivity and diffusivity of carbon-reinforced polyetherketoneketone composites. J Appl Polym Sci 2019;136(38):47975. https://doi.org/10.1002/app.47975.